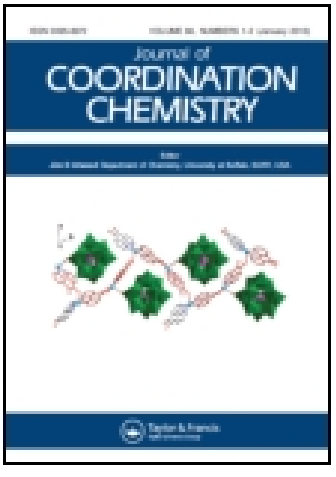


Journal of Coordination Chemistry
Publication details, including instructions for authors and subscription information:
http://www.tandfonline.com/loi/gcoo20

# Synthesis, structure, protein binding, and cytotoxicity of zinc(II) complexes with tridentate NNO Schiff-base ligands

Mei Li[ab], Yi Gou[b], Yao Zhang[b], Feng Yang[b] & Hong Liang[ab]

[a] College of Chemistry and Chemical Engineering, Central South University, Changsha, China

[b] State Key Laboratory Cultivation Base for the Chemistry and Molecular Engineering of Medicinal Resources, Ministry of Science and Technology of China, Guangxi Normal University, Guilin, China

Accepted author version posted online: 12 Mar 2014.Published online: 08 Apr 2014.



To cite this article: Mei Li, Yi Gou, Yao Zhang, Feng Yang & Hong Liang (2014) Synthesis, structure, protein binding, and cytotoxicity of zinc(II) complexes with tridentate NNO Schiff-base ligands, Journal of Coordination Chemistry, 67:6, 929-942, DOI: 10.1080/00958972.2014.903328

To link to this article: http://dx.doi.org/10.1080/00958972.2014.903328

*Journal of Coordination Chemistry*, 2014
Vol. 67, No. 6, 929–942, http://dx.doi.org/10.1080/00958972.2014.903328





# Synthesis, structure, protein binding, and cytotoxicity of zinc(II) complexes with tridentate NNO Schiff-base ligands

MEI LI†‡, YI GOU‡, YAO ZHANG‡, FENG YANG*‡ and HONG LIANG*†‡

†College of Chemistry and Chemical Engineering, Central South University, Changsha, China
‡State Key Laboratory Cultivation Base for the Chemistry and Molecular Engineering of Medicinal Resources, Ministry of Science and Technology of China, Guangxi Normal University, Guilin, China

(*Received 11 November 2013; accepted 18 February 2014*)

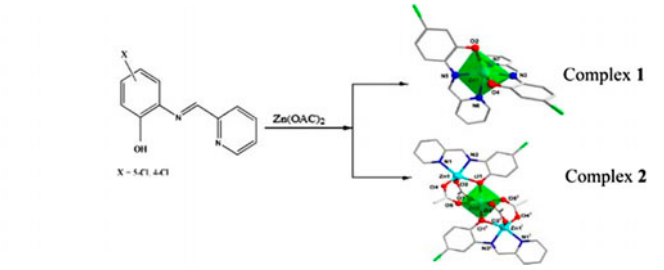


Mononuclear and trinuclear zinc(II) complexes (**1** and **2**) with tridentate NNO Schiff-base ligands ($HL^1$ = N-2-pyridiylmethylidene-4-chloro-2-hydroxy-phenylamine, $HL^2$ = N-2-pyridiylmethylidene-2-hydroxy-5-chloro-phenylamine) have been synthesized and characterized by single-crystal X-ray diffraction and elemental analysis. The binding properties of zinc(II) complexes with calf thymus DNA (CT-DNA) and HSA were investigated by UV–visible, fluorescence, and circular dichroism spectra. The zinc(II) complexes bind significantly to CT-DNA by intercalation and bind to protein HSA through a static quenching mechanism. The *in vitro* cytotoxicity of the complexes on human tumor cells lines was assessed by 3-(4,5-dimathylthiazol-2-yl)-2,5-diphenyl-tetrazolium bromide, Hoechst 33258 staining experiments.

*Keywords*: Zinc(II) complexes; NNO Schiff-base ligand; DNA and HSA binding; Anticancer activity

## 1. Introduction

Cisplatin and related platinum-based drugs are far from ideal anticancer agents due to their serious side effects, such as general toxicity and acquired drug resistance [1–4]. The main cellular target for platinum drugs is genomic DNA, in case of cisplatin the major antitumor activity results from intrastrand cross-links and the formation of DNA kinks [5]. To circumvent

*Corresponding authors. Email: jxyangfeng@gmail.com (F. Yang); hliang@mailbox.gxnu.edu.cn (H. Liang)

these problems, developing more effective, less toxic, target specific, and preferably non-covalently bound anticancer drugs would be of importance. Zinc is the second most abundant transition metal in living organisms after iron and the only metal that appears in all enzyme classes and is essential for growth and development of various biological systems due to its redox inertness, low toxicity, hard Lewis acid properties, and bioavailability. Hence, efficient zinc(II)-based hydrolytic cleavage agents may be candidates with better applications at the cellular level and constitute a remarkable achievement particularly for biomedical applications [6, 7]. However, it is a pity that very little data exist on the cytotoxicity of zinc-based compounds [8–13].

NNO Schiff-base ligands derived from pyridine-2-aldehyde and substituted 2-aminophenol have rich coordination chemistry and their metal complexes show unique properties as solid materials [14–16]. Few studies on biological activities of their metal complexes have been reported [17]. To widen the scope of investigations on new biologically active pharmaceuticals of zinc(II) complexes, in this work, two new zinc complexes containing tridentate NNO Schiff-base ligands have been obtained, and the complex-DNA binding, complex-HSA binding, and cytotoxicity *in vitro* have been studied.



## 2. Experimental

### 2.1. *Materials and physical measurements*

All chemicals were commercially available and used without purification. 2-Amino-4-chlorophenol, 2-amino-5-chlorophenol, and pyridine-2-aldehyde were purchased from Alfa Aesar Chemicals Co. (USA). Ethidium bromide (EB), HSA, calf thymus DNA (CT-DNA), 3-(4,5-dimethylthiazol-2-yl)-2,5-diphenyl-tetrazolium bromide (MTT), and Hoechst 33258 were purchased from Sigma (USA). Fetal bovine serum (FBS) and RPMI 1640 were obtained from Hyclone (USA). The Tris–HCl buffer solution was prepared with triply-distilled water.

Elemental analyses (C, H, and N) were carried out on a Perkin-Elmer Series II CHNS/O 2400 elemental analyzer. Infrared spectra were obtained on a Perkin-Elmer FT-IR spectrometer. Electrospray ionization mass spectrum (ESI-MS) was recorded on a Bruker HCT Electrospray Ionization Mass Spectrometer. UV–visible (UV–vis) absorption spectra were performed on a Varian Cary100 UV–vis spectrophotometer. Fluorescence measurements were obtained using a Shimadzu RF-5301/PC spectrofluorophotometer. The circular dichroic spectra of CT-DNA were performed on a JASCO J-810 automatic recording spectropolarimeter operating at 25 °C.

### 2.2. *Synthesis of $HL^1$ and $HL^2$*

**2.2.1. $HL^1$.** N-2-pyridiylmethylidene-4-chloro-2-hydroxy-phenylamine was prepared by refluxing equimolar amounts of pyridine-2-carbaldehyde (0.96 mL, 10 mM) and 2-amino-5-chlorophenol (1.44 g, 10 mM) in anhydrous methanol (60 mL) for 4 h with stirring. After solvent was removed under reduced pressure, the product was recrystallized from 30 mL n-hexane-$CH_2Cl_2$ (v : v = 1 : 1) and yellow crystals were collected from the filtrate. Yield: 1.65 g, 70.21%. FT-IR bands (KBr, $cm^{-1}$): 1628, (C=N); 3100–3000, (–OH). ESI-MS (in DMSO): *m/z* 231.7 (Calcd 232.67). Elemental analysis (%): Calcd for $C_{12}H_9ClN_2O$ (Mr = 232.67): C, 61.89; H, 3.87; N, 12.03. Found: C, 61.70; H, 3.81; N, 11.93.

**2.2.2. $HL^2$.** N-2-pyridiylmethylidene-2-hydroxy-5-chlorophenylamine was prepared according to a previously reported procedure [18] and yellow crystals were collected from the filtrate.

### 2.3. *Synthesis of 1 and 2*

**2.3.1. Complex 1.** To a yellow solution of $HL^1$ for **1** (0.046 g, 0.2 mM) in MeOH (12 mL) was added a methanolic solution (8 mL) of $Zn(OAc)_2 \cdot H_2O$ (0.037 g, 0.2 mM) dropwise with stirring for 2 h. The red reaction mixture was filtered and left to stand at room temperature for slow evaporation, and the red crystals of complexes suitable for X-ray analysis were harvested after several days. Yield: 0.056 g, 68.29%. Elemental analysis (%): Calcd for $C_{24}H_{16}Cl_2N_4O_2Zn$ (Mr = 528.70): C, 54.47; H, 3.03; N, 10.59. Found: C, 54.59; H, 3.01; N, 10.43.

**2.3.2. Complex 2.** Complex **2** was synthesized according to the above-described procedure using $HL^2$ instead of $HL^1$. The red crystals suitable for X-ray analysis were harvested after several days. Yield: 0.043 g, 52%. Elemental analysis (%): Calcd for $C_{32}H_{32}Cl_2N_4O_{12}Zn_3$ (Mr = 899.87): C, 42.67; H, 3.56; N, 6.22. Found: C, 42.59; H, 3.51; N, 6.23.

The outline of the synthesis of the two complexes is given in scheme 1.

### 2.4. *X-ray crystallography*

X-ray diffraction data for the complexes were collected on a Bruker Smart Apex II CCD diffractometer equipped with graphite-monochromated Mo Kα radiation ($\lambda = 0.71073$) at room temperature. The structures were solved with direct methods and refined using *SHELX*-97 [19, 20]. The non-hydrogen atoms were located in successive difference Fourier synthesis. The final refinement was performed by full-matrix least squares methods with anisotropic thermal parameters for non-hydrogen atoms on $F^2$. The hydrogens were added theoretically, riding on the concerned atoms.

### 2.5. *DNA-binding experiments*

DNA absorbs at 260 nm; protein absorbs at 280 nm. The concentration of CT-DNA was determined from its absorption intensity at 260 nm, taking the molar extinction coefficient of 6600 $M^{-1}$ $cm^{-1}$ [21]. The absorbance at 260 nm (A260) and at 280 nm (A280) for CT-DNA was measured to check its purity. The ratio A260/A280 was 1.8–1.9 in Tris–HCl/NaCl buffer (pH 7.2, 5 mM Tris–HCl, 50 mM NaCl), indicating that the DNA was sufficiently free of protein [22]. The $2 \times 10^{-3}$ M CT-DNA stock solution was stored at 4 °C for no more than 4 days before use. Complexes **1** and **2** were prepared as $2 \times 10^{-3}$ M DMSO stock solutions and diluted by Tris–HCl/NaCl buffer for DNA-binding studies. Absorption titration experiments were carried out with fixed concentrations of **1** and **2** ($2 \times 10^{-5}$ M) with varying concentrations of CT-DNA (0–140 μM). After the mixture was incubated for 5 min, absorption spectra were recorded.

EB displacement experiments were determined with an EB-bound CT-DNA solution by the fluorescence spectral method. Thus, aliquots of a solution of **1** and **2** were added to a solution of EB-bound CT-DNA ([EB] = $2 \times 10^{-5}$ M, [CT-DNA] = $8 \times 10^{-5}$ M) in Tris–HCl/

NaCl buffer. The corresponding fluorescence intensities at 602 nm (excitation at 350 nm) were obtained.

The circular dichroism (CD) spectra of CT-DNA in the absence and presence of **1** and **2** were collected in Tris–HCl buffer (pH 7.2) containing 50 mM NaCl from 350 to 230 nm at 25 °C.

### 2.6. *Cell culture*

The tumor cell line HepG2 (human liver hepatocellular carcinoma cells) was obtained from the American Type Culture Collection (Rockville, MD, USA). Cells were cultured in a humidified atmosphere containing 5% $CO_2$ at 37 °C in RPMI-1640 medium supplemented with 100 μg $mL^{-1}$ streptomycin and 100 units $mL^{-1}$ penicillin, 10% FBS.

### 2.7. *Cytotoxicity evaluation*

Cell viability was calculated in growth inhibition assays with exposure to drugs [23]. Cells were seeded at a density of $1 \times 10^4$ cells per well in 96-well plates and cultured for 24 h. Different concentrations of the complexes between 0 and 160 μM were added and the plates were incubated in a 5% $CO_2$ humidified atmosphere for 48 h. Then, 10 μL of 5 mg $mL^{-1}$ MTT in phosphate buffered saline (PBS; pH 7.40) was added to each well, and cells were incubated at 37 °C for an additional 4 h. The addition of 100 μL of DMSO dissolved formed formazan crystals and the absorbance at 570 nm was recorded by an enzyme-linked immunosorbent assay reader. The cytotoxicities of the complexes against tumor cell lines were determined according to $IC_{50}$ values which were expressed by plotting the percentage viability *versus* concentration on a logarithmic graph and reading off the concentration at which 50% of cells were viable relative to the control.

### 2.8. *Hoechst 33258 staining*

The nuclear morphology of cells was employed to detect early apoptosis, late apoptosis, and necrosis. HepG2 cells were seeded in a 6-well plate at a density of $5 \times 10^5$ well and incubated for 24 h. Then, various concentrations of complexes (0, 10, 20, and 40 μM) were added to the media and cells were cultured for another 24 h. Then, cells were washed with PBS and stained with Hoechst 33258 for 5 min at 25 °C. After a final wash in PBS, samples were measured with the aid of EPI fluorescence microscopy (Nikon MF30 LED, Japan).

### 2.9. *Interaction with HSA*

The interactions of **1** and **2** with HSA were carried out using fluorescence spectra. Various concentrations of complexes ($0–12 \times 10^{-5}$ M) were added to a solution containing $1 \times 10^{-6}$ M HSA and 20 mM NaCl/Tris–HCl buffer (pH 7.4). Fluorescence spectra were obtained by recording the emission spectra (260–500 nm) corresponding to excitation at 280 nm.

## 3. Results and discussion

### 3.1. *Description of the structures*

Complexes **1** and **2** were prepared by the same procedure (scheme 1) except using 2-amino-4-chlorophenol instead of 2-amino-5-chlorophenol. Complexes **1** and **2** are red, but the yields are different, **1** (68.29%) > **2** (52%). The replacement of 4-chloro by 5-chloro in the ligands resulted in change in reactivity of the ligands and led to different yields [24]. To characterize the bis-Schiff-base Zn(II) complexes and study their geometries with different anions, X-ray crystal structures of the bis-Schiff-base complexes were determined. The X-ray crystal structures of **1** and **2** are shown in figures 1 and 2. The details of crystallographic data and structure refinement parameters are summarized in table 1. Selected bond distances and angles for the structures of **1** and **2** are listed in table 2. X-ray diffraction reveals that **1** crystallizes in a triclinic system with space group *P-1*, while **2** crystallizes in a monoclinic system with space group $P2_1/n$.

Complex **1** has two meridional Schiff-base ligands with pseudo-octahedral coordination geometry [figure 1(A)]. The coordination geometry about Zn(II) is rather irregular, and the relative deviations of bond lengths and angles from the ideal values (table 2) also support the distorted geometry of the zinc(II) center. The two tridentate Schiff-base ligands are almost planar and perpendicular (ca. 88.95°) to one another [figure 1(B)]. The bond lengths with average Zn1–O at 2.086 Å and Zn1–N at 2.221 Å are consistent with other complexes [25, 26]. Trans angles (within the meridional ligands) for the Zn(II) complex are O2–Zn1–N6 = 151.774° and O4–Zn1–N7 = 152.624(2)° with an interligand trans angle of 165.349° for N3–Zn1–N5.

In contrast to **1**, **2** displays a trinuclear molecule with a central Zn(II) lying on a center of inversion. The trinuclear complex is built up of two mononuclear ZnL moieties, which are linked through bridging carboxylates and $\mu^2$-groups to the central Zn [figure 2(A)]. The coordination geometry around the terminal Zn centers may be regarded as distorted square pyramidal, described by the $\tau$ value 0.34 [27], and at the lower end of the range (0.32–0.45) for similar Zn(II) complexes [28–30]. However, the central zinc resides on a center of symmetry and is surrounded by O6 donor set composed of four oxygens (Zn2–O3/O3$^i$, 2.218 Å; Zn2–O5/O5$^i$, 2.118 Å) of four bridging $OAc^-$ (*syn–syn* mode) and two phenolic oxygens (Zn2–O1/O1$^i$, 2.071 Å) of two Schiff bases to form an octahedral structure (Zn1–Zn2–Zn1$^i$ = 180.00°). The distance between the central zinc ion (Zn2) and the two terminal zincs is 3.3555 Å, which is in the expected range for a carboxylate bridged metal–metal

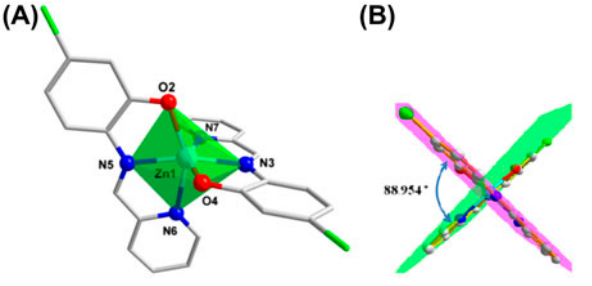


Figure 1. (A) Crystal structure of **1**. Hydrogens are omitted for clarity. (B) The angle of two planar tridentate Schiff-base ligands in **1**.

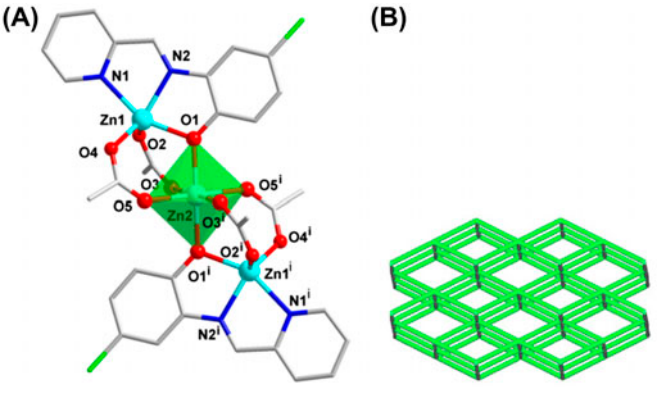


Figure 2. (A) Crystal structure of **2**. Hydrogens and $H_2O$ are omitted for clarity (symmetry code: $1-x$, $1-y$, $1-z$). (B) Schematic representation of the 6-connected α–Po topological net of **2**.

Table 1. Crystallographic data and structure refinement parameters for **1** and **2**.

| | **1** | **2** |
|---|---|---|
| Empirical formula | $C_{24}H_{16}Cl_2N_4O_2Zn$ | $C_{32}H_{32}Cl_2N_4O_{12}Zn_3$ |
| Formula weight | 528.70 | 899.87 |
| Temperature/K | 296(2) | 293(2) |
| Crystal system | Triclinic | Monoclinic |
| Space group | *P-1* | $P2_1/n$ |
| *a*/Å | 8.008(4) | 8.9794(9) |
| *b*/Å | 12.084(7) | 20.3939(16) |
| *c*/Å | 13.133(7) | 10.2034(12) |
| *α*/° | 115.113(8) | 90.00 |
| *β*/° | 100.271(9) | 106.109(11) |
| *γ*/° | 99.708(9) | 90.00 |
| Volume/Å$^3$ | 1088.9(10) | 1795.1(3) |
| *Z* | 2 | 2 |
| $\rho_{Calcd}$/mg mm$^{-3}$ | 1.612 | 1.665 |
| $\mu$/mm$^{-1}$ | 1.404 | 2.203 |
| *F* (0 0 0) | 552 | 881 |
| Crystal size/mm$^3$ | 0.35 × 0.25 × 0.11 | 0.20 × 0.08 × 0.05 |
| 2Θ range for data collection | 1.78–26.37° | 5.72–52.74° |
| Index ranges | $-10 \le h \le 10$, $-15 \le k \le 15$, $-16 \le l \le 16$ | $-11 \le h \le 11$, $-25 \le k \le 24$, $-12 \le l \le 10$ |
| Reflections collected | 12,422 | 9606 |
| Independent reflections | 4429 [*R*(int) = 0.0915] | 3670 [*R*(int) = 0.0844] |
| Data/restraints/parameters | 4429/0/298 | 3670/3/249 |
| Goodness-of-fit on $F^2$ | 1.150 | 1.015 |
| Final *R* indexes [$I > 2\sigma(I)$] | $R_1 = 0.0781$, $wR_2 = 0.1931$ | $R_1 = 0.0702$, $wR_2 = 0.1134$ |
| Final *R* indexes [all data] | $R_1 = 0.1300$, $wR_2 = 0.2226$ | $R_1 = 0.1393$, $wR_2 = 0.1431$ |
| Largest diff. peak/hole/e Å$^{-3}$ | 1.404/−1.665 | 0.709/−0.679 |

entity. These Zn–Zn distances are longer than that (3.3420 Å) observed for the linear trinuclear zinc(II) complex, $[Zn_3L_2(CH_3COO)_4]$ [30], where L denotes [C5H4NC(CH3)=NC6H4($O^-$)]. There exist three weak interactions: O–H···O hydrogen bond interactions involving the uncoordinated $H_2O$ and a coordinated carboxyl oxygen (O3) [O6···O3 = 3.089 Å]; O–H···Cl hydrogen bond interactions between the adjacent molecules (O6···Cl1 = 3.198 Å and the O6–H6A···Cl1 angle is 112.4°); and O···O interactions (O6···$O6^i$ = 2.854 Å). When above weak interactions are taken into account, the resulting structure

Table 2. Selected bond lengths (Å) and angles (°) for **1** and **2**.

| | | | |
|---|---|---|---|
| **1** | | | |
| Zn1–O2 | 2.097(4) | Zn1–N5 | 2.134(5) |
| Zn1–N3 | 2.133(5) | Zn1–N6 | 2.315(5) |
| Zn1–O4 | 2.075(4) | Zn1–N7 | 2.263(6) |
| O2–Zn1–N3 | 115.05(18) | N3–Zn1–N6 | 91.68(18) |
| O2–Zn1–N5 | 78.63(18) | N3–Zn1–N7 | 74.00(18) |
| O2–Zn1–N6 | 151.76(19) | N3–C11–C8 | 113.4(5) |
| O2–Zn1–N7 | 91.17(19) | N3–C12–C13 | 118.3(6) |
| O2–C9–C14 | 121.9(5) | O4–Zn1–O2 | 99.03(19) |
| O2–C9–C20 | 121.4(6) | O4–Zn1–N3 | 78.68(17) |
| N3–Zn1–N5 | 165.35(18) | O4–Zn1–N5 | 105.26(18) |
| O4–Zn1–N6 | 94.88(18) | N5–Zn1–N6 | 74.03(19) |
| O4–Zn1–N7 | 152.63(18) | N5–Zn1–N7 | 101.62(18) |
| **2** | | | |
| Zn1–O1 | 2.087(4) | Zn2–O1 | 2.070(4) |
| Zn1–O4 | 1.930(5) | Zn2–O3 | 2.128(4) |
| Zn1–N2 | 2.073(5) | Zn2–O5 | 2.119(5) |
| O1–Zn1–N1 | 153.96(19) | N2–Zn1–N1 | 75.9(2) |
| O2–Zn1–O1 | 103.23(18) | O5–Zn2–O3 | 93.8(2) |
| O2–Zn1–N1 | 90.33(19) | Zn2–O1–Zn1 | 107.65(19) |
| O2–Zn1–N2 | 113.6(2) | C1–N1–C5 | 118.1(6) |
| O4–Zn1–O1 | 99.87(19) | C5–N1–Zn1 | 112.8(4) |
| O4–Zn1–O2 | 112.2(2) | C6–N2–Zn1 | 118.5(4) |
| O4–Zn1–N1 | 95.2(2) | C6–N2–C7 | 127.5(6) |
| O4–Zn1–N2 | 133.3(2) | C7–N2–Zn1 | 113.9(4) |
| N2–Zn1–O1 | 78.30(18) | O1–Zn2–O5 | 88.31(19) |

displays a 3D 6-connected net with α–Po ($4^{12}6^3$) topology [figure 2(B)]. A distorted cube-like unit of the resulting α–Po net shows dimensions of 11.724 × 11.724 × 10.203 Å.

### 3.2. *Interaction with CT-DNA*

**3.2.1. Absorption spectral studies.** DNA binding is the critical step for DNA cleavage in most cases [31–33]. Therefore, the binding ability of complexes to CT-DNA was studied by using UV–vis absorption and fluorescence spectroscopy. The typical titration curves for **1** and **2** are shown in figure 3. The absorption peaks of both complexes at 268 and 370 nm are attributed to intraligand π–π* transition; with increasing the CT-DNA concentrations, hypochromism of 11.0% at 268 nm and 12.6% at 370 nm for **1**, hypochromism of 10.3% at 268 nm and 11.9% at 370 nm for **2**, and a slight redshift for both complexes are observed. These results suggest intercalation between the complexes and DNA, because intercalation would give hypochromism and bathochromism in UV absorption spectra due to the intercalative mode involving a strong stacking interaction between an aromatic chromophore and the base pairs of DNA [34]. The extent of the hypochromism commonly reflects the strength of intercalative interaction [35]. The intrinsic binding constant $K_b$ was determined from a plot of [DNA]/($\varepsilon_a - \varepsilon_f$) *versus* [DNA] using the equation: [DNA]/($\varepsilon_a - \varepsilon_f$) = [DNA]/($\varepsilon_b - \varepsilon_f$) + 1/$K_b$($\varepsilon_b - \varepsilon_f$), where [DNA] is the concentration of DNA in base pairs. The apparent absorption coefficients $\varepsilon_a$, $\varepsilon_f$, and $\varepsilon_b$ correspond to $A_{obsd.}$/[complex], the extinction coefficient for the free complex and extinction coefficient for the complex in the fully bound form, respectively [36]. $K_b$ is given by the ratio of slope to intercept. From absorption data, the binding constant $K_b$ for **1** is $1.4 \times 10^3\ M^{-1}\ M^{-1}$ and for **2** is $1.2 \times 10^3\ M^{-1}$, lower than

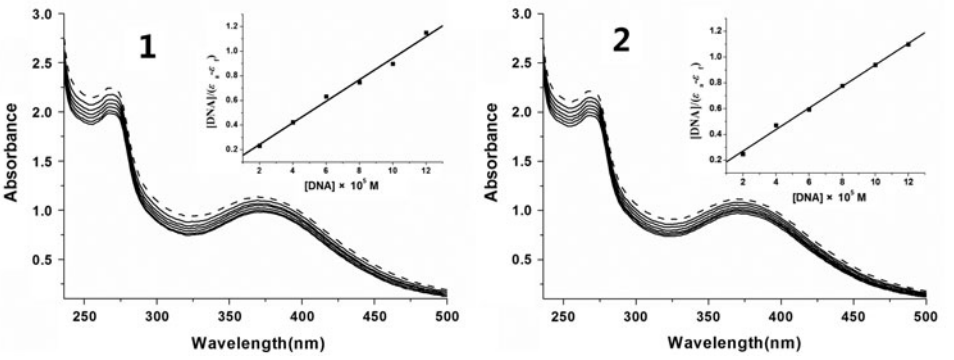


Figure 3. Absorption spectra of **1** and **2** ([complex] = $2.0 \times 10^{-5}$ M) in the absence (dashed line) and presence (solid line) of increasing amounts of CT-DNA from 1 : 1 to 7 : 1.

those observed [37–41] for the classical intercalator EB ($K_b$, $4.94 \times 10^5$ $M^{-1}$ in a 25 mM Tris–HCl/40 mM NaCl buffer, pH 7.9). The results suggest that interaction of the two complexes with DNA is weak intercalation; the lower $K_b$ of **2** than **1** indicates steric hindrance has an effect on the interaction with DNA.

**3.2.2. Fluorescence quenching studies.** Competitive binding was carried out to further clarify the interaction of the complex with DNA. EB emission fluorescence intensity at 600 nm in the presence of DNA is due to its strong intercalation between adjacent DNA base pairs [42, 43]. It was previously reported that addition of another molecule could quench the enhanced fluorescence. This reduction in the emission intensity may be ascribed to replacement of molecular fluorophores and/or electron transfer [44, 45]. The relative binding of **1** and **2** to CT-DNA was studied with an EB-bound CT-DNA solution in 5 mM Tris–HCl/50 mM NaCl buffer (pH 7.2). The fluorescence spectra of EB-bound CT-DNA are similar in **1** and **2**. The result of **2** is shown in figure 4(A). In fluorescence spectra, the

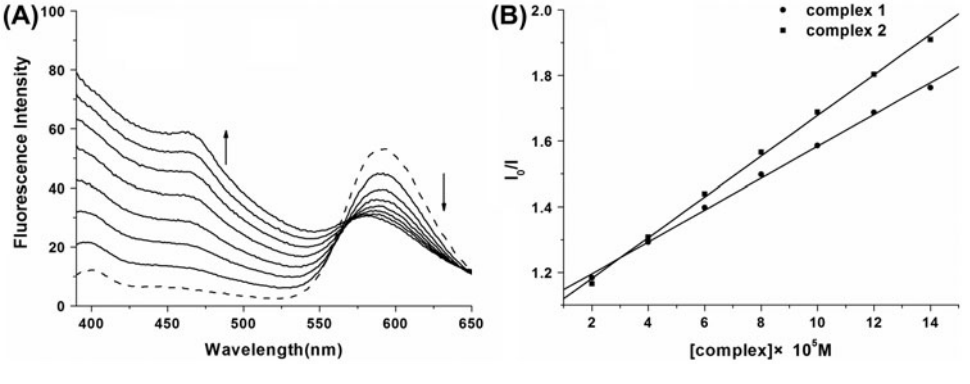


Figure 4. (A) Fluorescence quenching curves of EB bound to DNA by **2** [complex] = 0–$14 \times 10^{-5}$ M). The arrow shows the intensity changes on increasing the complex concentration. (B) Plot of I0/I *vs.* [complex] for the titration of complexes to EB-bound CT-DNA.

addition of **1** and **2** to solution of EB-DNA induced a decrease in the fluorescence intensity at 590 nm (350 nm excitation). The extent of reduction in the emission intensity measures the binding propensity of the complex to DNA [figure 4(A)]. The relative binding intensity of **1** and **2** to CT-DNA was determined by the classical Stern–Volmer equation: $I_0/I = 1 + K$ [Q], where $I_0$ and $I$ are the fluorescence intensities in the absence and presence of complex, respectively, $K$ is a linear Stern–Volmer constant, and [Q] is the concentration of complex to that of DNA. $K$ was calculated from the slope of a plot of $I_0/I$ *versus* [Q] [46]. The apparent binding constants $K$ of **1** and **2** at 25 °C were calculated to be $6.20 \times 10^4\ M^{-1}$ and $4.85 \times 10^4\ M^{-1}$, respectively [figure 4(B)]. The binding constants of the classical intercalators and metallointercalators were in the order of $10^7\ M^{-1}$ [47]. The results suggest that **1** and **2** interact with DNA through intercalation, releasing some free EB from the EB-DNA complex, consistent with the above absorption spectral results.

**3.2.3. CD spectral studies.** CD spectroscopy is useful in monitoring the conformational variations of DNA in solution. The CD spectra of CT-DNA exhibit a positive band at 275 nm due to base stacking and a negative band at 245 nm due to the helicity of B-type DNA [48]. While groove binding interaction of small molecules with DNA shows little or no perturbations on the base stacking and helicity bands, intercalation enhances the intensities of both bands, stabilizing the right-handed B conformation of CT-DNA. Figure 5 displays the CD spectra of CT-DNA with and without **1** and **2**. In the presence of complexes, both the positive (~275 nm) and negative (~245 nm) bands decreased in intensity, clearly indicating interactions between the complexes and DNA. The decreased intensity in the negative band suggests the complex can unwind the DNA helix and lead to loss of helicity [49].

### 3.3. *MTT assay*

The cytotoxicity of zinc complexes against HepG2 was estimated by MTT assay. The growth inhibition of HepG2 cells with the chemicals is $IC_{50} = 40 \pm 1$ μM (**1**), $20 \pm 2$ μM (**2**),

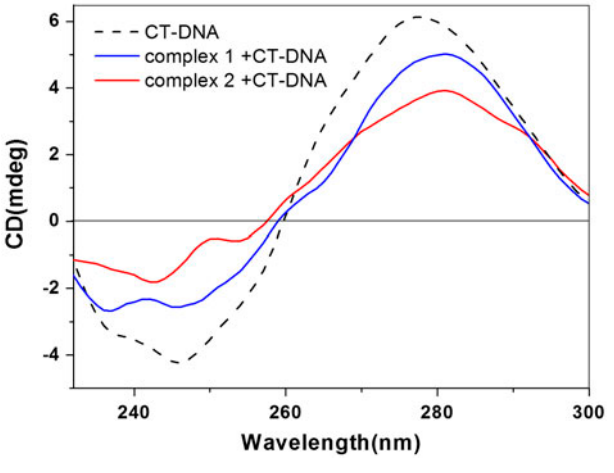


Figure 5. CD spectra of CT-DNA (3 mL solution, $2.0 \times 10^{-4}$ M) in the absence (dashed line) and presence of complexes (solid line), with [compound]/[CT-DNA] = 0.25 in Tris–HCl buffer, pH 7.2.

$102 \pm 2\,\mu M$ ($HL^2$), and $1000.97\,\mu M$ ($Zn(OAc)_2$), respectively. The results showed that **2** derived from pyridine-2-aldehyde and 2-amino-4-chlorophenol was essential for anticancer activities and $Zn(OAc)_2$ could not inhibit proliferation of HepG2 cells. Cell growth inhibition activity by zinc complex must be derived from biological activities of this zinc complex, not simply from free zinc chaperoned into the cells by the ligand.

### 3.4. *Apoptosis evaluation*

Apoptosis can be identified by visualizing nuclear changes and apoptotic body formation. From the results of MTT assay, **2** was selected for this apoptosis evaluation. HepG2 cells were treated with **2** at various concentrations for 24 h, stained with Hoechst 33258 [50, 51]. As shown in figure 6, Hoechst 33258 staining showed blue apoptotic cells with apoptotic features that exhibit nuclear pyknosis, showing round shapes and an enhanced fluorescent signal. The results show that **2** can induce apoptosis of HepG2 cells.

### 3.5. *Interaction with HSA*

Interaction between serum albumin and compounds is important in drug transport and drug metabolism functions of HSA [52, 53]. The fluorescence of HSA comes from tryptophan, tyrosine, and phenylalanine residues. Phenylalanine has a very low quantum yield and fluorescence of a tyrosine ionized is almost completely quenched; the intrinsic fluorescence of many proteins is mainly contributed by tryptophan alone.

The fluorescence emission of HSA tryptophan residues was similar in the presence of **1** and **2**. The result of **2** is shown in figure 7. With increasing concentrations of the complexes, the intensity of the characteristic fluorescence emission band at 342 nm decreases regularly, which indicates that interaction has occurred between the complex and HSA. The fluorescence quenching is described according to the Stern–Volmer equation, $F_0/F = 1 + Kq\,\tau_0[Q] = 1 + K_{SV}[Q]$, where $F_0$ and $F$ represent the fluorescence intensities in the absence and in the presence of quencher, $Kq$ is the quenching rate constant, $\tau_0$ is the average lifetime of the biomolecule without quencher (about $10^{-8}$ s) [53], $K_{SV}$ is the Stern–Volmer quenching constant, and [Q] is the concentration of quencher. Figure 8(A) displays the Stern–Volmer plots of the quenching of HSA fluorescence by the complexes, and $K_{SV}$ can be obtained by a slope from the plot of $F_0/F$ *versus* [Q]. The calculated values of $K_{SV}$ and $Kq$ for interaction of the complexes with HSA are $1.02 \times 10^5\,M^{-1}$ and $1.02 \times 10^{13}\,M^{-1}\,s^{-1}$ for **1**, $0.84 \times 10^5\,M^{-1}$ and $0.84 \times 10^{13}\,M^{-1}\,s^{-1}$ for **2**, respectively. The results indicate that **1** and **2** quench the fluorescence intensity of HSA.

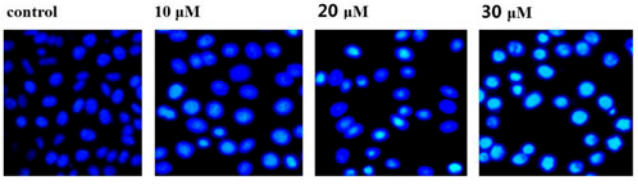


Figure 6. Apoptosis of HepG2 cells induced by the complex. Morphological changes of HepG2 cells treated with various concentrations of **2** (10, 20, and 30 μM) for 24 h. Hoechst 33258 staining.

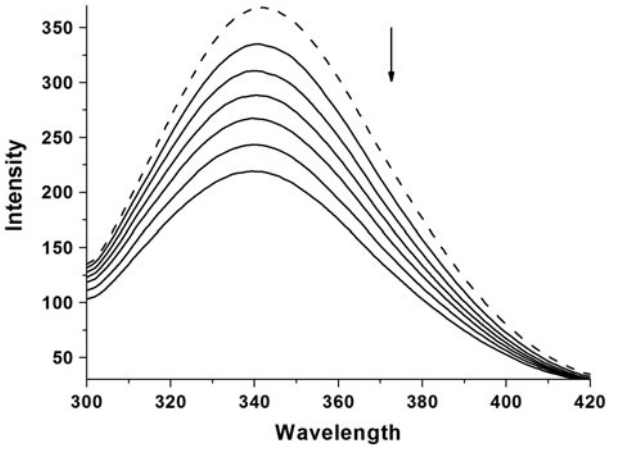


Figure 7. Fluorescence emission spectra of the HSA (2 μM) system in the absence (dashed line) and presence (solid lines) of **2** (2, 4, 6, 8, 10, and 12 μM).

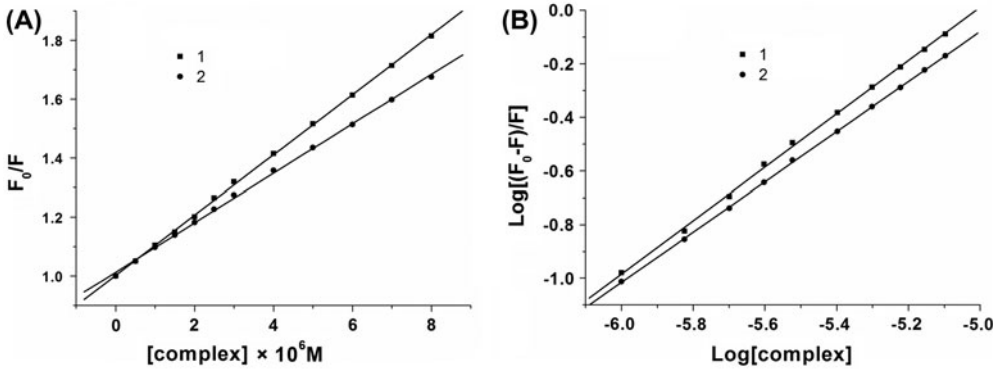


Figure 8. (A) Plot of $F_0/F$ *vs.* [complex] for the titration of the complex to HSA. (B) Plot of $\log[(F_0 - F)/F]$ *vs.* log[complex] for the titration of the complex to HSA.

Quenching mechanisms are usually dynamic quenching or static quenching. The process of dynamic quenching occurs when the fluorophore and the quencher collide during the transient existence of the exited state. Static quenching refers to fluorophore–quencher complex formation. Compared with the maximum scatter collision-quenching constant of biopolymers fluorescence ($2 \times 10^{10}\,M^{-1}\,s^{-1}$), *K*q values of the complexes are higher, indicating the existence of a static quenching mechanism [54].

For static quenching interaction, the binding constant ($K$) and the number of binding sites ($n$) can be determined according to the Scatchard equation [55]: $\log(F_0 - F)/F = \log K + n \log[Q]$. The $n$ and $K$ (1.0 and $9.78 \times 10^4\,M^{-1}$ L for **1**, 0.9 and $4.01 \times 10^4\,M^{-1}$ L for **2**) can be determined by the slope and intercept of the double logarithm regression curve of log $(F_0 - F)/F$ *versus* log[Q] [figure 8(B)], which show **1** and **2** exhibit higher binding constants for HSA.

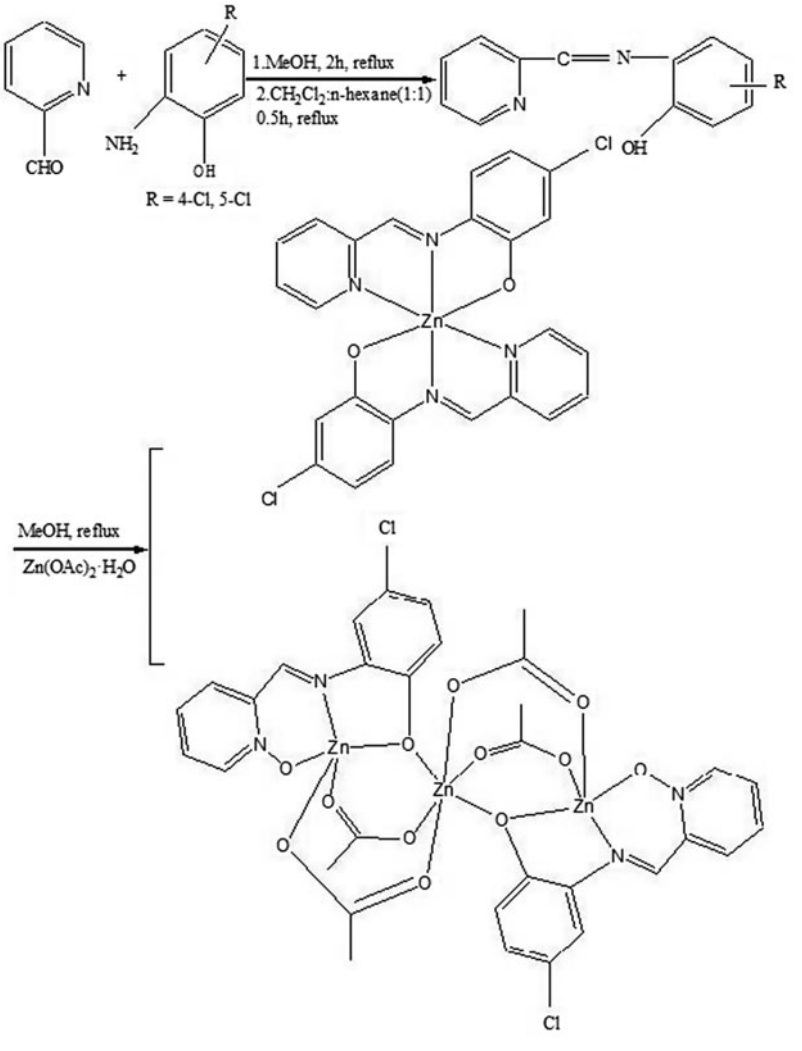


Scheme 1. The synthesis of complexes.

## 4. Conclusion

Two zinc(II) complexes have been prepared and characterized structurally. The reactivity toward CT-DNA and protein HSA reveal that **1** and **2** can interact with CT-DNA by intercalation, and **1** and **2** bind to HSA which is responsible for quenching of tryptophan fluorescence by static quenching. The zinc(II) complexes are cytotoxic to HepG2 cells, the mechanism of cell death appears to be apoptosis. Our results found that zinc(II) complexes may prove to be anticancer drugs, possibly targeting DNA and inducing apoptosis in the selected cancer cell lines.

## Supplementary material

Crystallographic data for the structures reported in this article have been deposited with the Cambridge Crystallographic Data Center, CCDC No. 964990 for **1** and 959446 for **2**. Copies of this information may be obtained free of charge from the Director, CCDC, 12 Union Road, Cambridge, CB2 1EZ, UK (Fax: +44-1223-336033; E-mail: deposit@ccdc.cam.ac.uk or http://www.ccdc.cam.ac.uk).



## Funding

This work was supported by the Natural Science Foundation of China [grant number 31060121], [grant number 21171043] and Natural Science Foundation of Guangxi [grant number 2012GXNSFCB053001].

## References

[1] B. Rosenberg, L. VamCamp, J.E. Trosko, V.H. Mansour. *Nature*, **222**, 385 (1969).
[2] F. Arnesano, G. Natile. *Coord. Chem. Rev.*, **253**, 2070 (2009).
[3] A.V. Klein, T.W. Hambley. *Chem. Rev.*, **109**, 4911 (2009).
[4] R. Gust, W. Beck, G. Jaouen, H. Schönenberger. *Coord. Chem. Rev.*, **253**, 2742 (2009).
[5] M. Mrksich, P.B. Dervan. *J. Am. Chem. Soc.*, **115**, 9892 (1993).
[6] M. Komiyama, N. Takeda, H. Shigekawa. *Chem. Commun.*, **82**, 1443 (1999).
[7] T. Niittymäki, H. Lönnberg. *Org. Biomol. Chem.*, **4**, 15 (2006).
[8] D. Miyamoto, N. Endo, N. Oku, Y. Arima, T. Suzuki, Y. Suzuki. *Biol. Pharm. Bull.*, **21**, 1258 (1998).
[9] M. Belicchi Ferrari, F. Bisceglie, G. Pelosi, P. Tarasconi, R. Albertini, S. Pinelli. *J. Inorg. Biochem.*, **87**, 137 (2001).
[10] H. Beraldo, D. Gambinob. *Mini-Rev. Med. Chem.*, **4**, 31 (2004).
[11] J. Tan, B. Wang, L. Zhu. *Bioorg. Med. Chem.*, **17**, 614 (2009).
[12] Q. Jiang, J. Zhu, Y. Zhang, N. Xiao, Z. Guo. *BioMetals*, **22**, 297 (2009).
[13] J.H. Wen, C.Y. Li, Z.R. Geng, X.Y. Ma, Z.L. Wang. *Chem. Commun.*, **47**, 11330 (2011).
[14] S. Das, S. Pal. *Inorg. Chim. Acta*, **363**, 3028 (2010).
[15] M. Wałęsa-Chorab, A. Gorczyński, M. Kubicki, Z. Hnatejko, V. Patroniak. *Polyhedron*, **31**, 51 (2012).
[16] S.E. Balaghi, E. Safaei, M. Rafiee, M.H. Kowsari. *Polyhedron*, **47**, 94 (2012).
[17] X. Qiao, Z.Y. Ma, C.Z. Xie, F. Xue, Y.W. Zhang, J.Y. Xu, Z.Y. Qiang, J.S. Lou, G.J. Chen, S.P. Yan. *J. Inorg. Biochem.*, **105**, 728 (2011).
[18] H. Asada, K. Hayashi, S. Negoro, M. Fujiwara, T. Matsushita. *Inorg. Chem. Commun.*, **6**, 193 (2003).
[19] G.M. Sheldrick. *SHELXS-97, Program of the Solution of Crystal Structure*, University of Göttingen, Germany (1997).
[20] G.M. Sheldrick. *SHELXL-97, Program of the Refinement of Crystal Structure*, University of Göttingen, Germany (1997).
[21] M.E. Reichmann, S.A. Rice, C.A. Thomas, P. Doty. *J. Am. Chem. Soc.*, **76**, 3047 (1954).
[22] J. Marmur. *J. Mol. Biol.*, **3**, 208 (1961).
[23] T. Mosmann. *J. Immunol. Methods*, **65**, 55 (1983).
[24] A.K. Asatkar, S. Nair, V.K. Verma, C.S. Verma, T.A. Jain, R. Singh, S.K. Gupta, R.J. Butcher. *J. Coord. Chem.*, **65**, 28 (2012).
[25] A.R. Stefankiewicz, M. Wałęsa-Chorab, H.B. Szcześniak, V. Patroniak, M. Kubicki, Z. Hnatejko, J. Harrowfield. *Polyhedron*, **29**, 178 (2010).
[26] D.M. Epstein, S. Choudhary, M.R. Churchill, K.M. Keil, A.V. Eliseev, J.R. Morrow. *Inorg. Chem.*, **40**, 1591 (2001).
[27] A.W. Addison, T.N. Rao, J. Reedijk, J. Van Rijn, G.C. Verschoor. *J. Chem. Soc., Dalton Trans.*, 1349 (1984).
[28] P. de Hoog, L.D. Pachon, P. Gamez, M. Lutz, A.L. Spek, J. Reedijk. *Dalton Trans.*, **17**, 2614 (2004).
[29] A. Majumder, G.M. Rosair, A. Mallick, N. Chattopadhyay, S. Mitra. *Polyhedron*, **25**, 1753 (2006).
[30] S. Shit, J. Chakraborty, B. Samanta, G.M. Rosair, S. Mitra. *Z. Naturforsch. Teil B*, **64**, 403 (2009).
[31] Y. Barenholz, J. Kasparkova, V. Brabec, D. Gibson. *Angew. Chem. Int. Ed.*, **44**, 2885e (2005).
[32] F. Arjmand, M. Aziz, M. Chauhan. *J. Inclusion Phenom. Macrocyclic Chem.*, **61**, 265 (2008).
[33] S.D.H. Abe, S. Aoyagi, C. Kibayashi, K.S. Gates. *J. Am. Chem. Soc.*, **127**, 15004 (2005).
[34] Z.C. Liu, B.D. Wang, Z.Y. Yang, Y. Li, D.D. Qin, T.R. Li. *Eur. J. Med. Chem.*, **44**, 4477 (2009).

[35] Z.C. Liu, B.D. Wang, B. Li, Q. Wang, Z.Y. Yang, T.R. Li, Y. Li. *Eur. J. Med. Chem.*, **45**, 5353 (2010).
[36] A. Wolfe, G.H. Shimer, T. Meehan. *Biochemistry*, **26**, 6392 (1987).
[37] D.L. Boger, B.E. Fink, S.R. Brunette, W.C. Tse, M.P. Hedrick. *J. Am. Chem. Soc.*, **123**, 5878 (2001).
[38] M. Jiang, Y.T. Li, Z.Y. Wu. *J. Coord. Chem.*, **65**, 1858 (2012).
[39] Y.F. Chen, M. Liu, J.W. Mao, H.T. Song, H. Zhou, Z.Q. Pan. *J. Coord. Chem.*, **65**, 3413 (2012).
[40] Y.J. Zheng, X.W. Li, Y.T. Li, Z.Y. Wu, C.W. Yan. *J. Coord. Chem.*, **65**, 3530 (2012).
[41] H.L. Wu, J.K. Yuan, Y. Bai, G.L. Pan, H. Wang, J.H. Shao, J.L. Gao, Y.Y. Wang. *J. Coord. Chem.*, **65**, 4327 (2012).
[42] F.J. Meyer-Almes, D. Porschke. *Biochemistry*, **32**, 4246 (1993).
[43] J.B. Lepecq, C. Paoletti. *J. Mol. Biol.*, **27**, 87 (1967).
[44] B.C. Baguley, M. Le Bret. *Biochemistry*, **23**, 937 (1984).
[45] R.F. Pasternack, M. Caccam, B. Keogh, T.A. Stephenson, A.P. Williams, E.J. Gibbs. *J. Am. Chem. Soc.*, **113**, 6835 (1991).
[46] M. Jiang, Y.T. Li, Z.Y. Wu. *J. Coord. Chem.*, **65**, 1858 (2012).
[47] J. Qian, L.P. Wang, W. Gu, X. Liu, J.L. Tian, S.P. Yan. *J. Coord. Chem.*, **64**, 2480 (2011).
[48] A. Rajendran, B.U. Nair. *Biochim. Biophys. Acta*, **1760**, 1794 (2006).
[49] A.D. Richards, A. Rodger. *Chem. Soc. Rev.*, **36**, 471 (2007).
[50] S. Dhar, D. Senapati, P.K. Das, P. Chattopadhyay, M. Nethaji, A.R. Chakravarty. *J. Am. Chem. Soc.*, **125**, 12118 (2003).
[51] D. Gibellini, F. Vitone, P. Schiavone, C. Ponti, M.L. Placa, M.C. Re. *J. Clin. Virol.*, **29**, 282 (2004).
[52] J.R. Lakowicz. *Principles of Fluorescence Spectroscopy*, 3rd Edn, Springer, New York, NY (2006).
[53] J.R. Lakowicz, G. Weber. *Biochemistry*, **12**, 4161 (1973).
[54] W.R. Ware. *J. Phys. Chem.*, **66**, 455 (1962).
[55] G. Scatchard, N.Y. Ann. *Acad. Sci.*, **51**, 660 (1949).